

# Coulomb Blockade Oscillations in Biological Ion Channels

I. Kh. Kaufman\*, W. Gibby\*, D. G. Luchinsky\*<sup>†</sup>, P. V. E. McClintock\*, R. S. Eisenberg<sup>‡</sup>

\*Department of Physics, Lancaster University, Lancaster LA1 4YB, UK

Email: p.v.e.mcclintock@lancaster.ac.uk

<sup>†</sup>Mission Critical Technologies Inc., 2041 Rosecrans Ave. Suite 225 El Segundo, CA 90245, USA

<sup>‡</sup>Department of Molecular Biophysics, Rush University, Chicago IL 60612, USA

**Abstract**—The conduction and selectivity of calcium/sodium ion channels are described in terms of ionic Coulomb blockade, a phenomenon based on charge discreteness, an electrostatic exclusion principle, and stochastic ion motion through the channel. This novel approach provides a unified explanation of numerous observed and modelled conductance and selectivity phenomena, including the anomalous mole fraction effect and discrete conduction bands. Ionic Coulomb blockade and resonant conduction are similar to electronic Coulomb blockade and resonant tunnelling in quantum dots. The model is equally applicable to other nanopores.

Biological ion channels are natural nanopores providing for the fast and highly selective permeation of physiologically important ions (e.g.  $\text{Na}^+$ ,  $\text{K}^+$  and  $\text{Ca}^{2+}$ ) through cellular membranes. [1]. The conduction and selectivity of e.g. voltage-gated  $\text{Ca}^{2+}$  [2] and  $\text{Na}^+$  channels [3] are defined by the ions' stochastic movements and interactions inside a short, narrow selectivity filter (SF) lined with negatively-charged protein residues<sup>1</sup> providing a net fixed charge  $Q_f$ . Permeation through the SF sometimes involves the concerted motion of more than one ion [4], [5]. Mutation studies [6], [7], [8], [3] and simulations [9], [10], [11] show that  $Q_f$  is a determinant of the channel's conductivity and valence selectivity. It has recently been shown that nanopores can exhibit ionic Coulomb blockade (CB) [12], a quantized electrostatic phenomenon equivalent to electronic CB in mesoscopic systems [13], [14], [15].

An electrostatic theory of ionic transport in water-filled periodically-charged nanopores revealed the phenomenon of ion-exchange through low-barrier phase transitions as the ion concentration and fixed charge  $Q_f$  were varied [16]. Comparable transitions in Brownian dynamics (BD) simulations of  $\text{Ca}^{2+}$  channels result in discrete conduction and selectivity bands as functions of  $Q_f$  [17], [18] consistent with earlier speculations [19], [14] and explaining both the anomalous mole fraction effect (AMFE) [2] and some of the puzzling mutation-induced transformations of selectivity in  $\text{Ca}^{2+}/\text{Na}^+$  channels [6], [3]. We have already connected the periodicity of the pattern of conduction bands with single/multi-ion barrier-less conduction and sequential neutralisation of the SF [18], but the shapes of the occupancy and conduction bands and the

<sup>1</sup>The protein residues are amino acids, of which aspartate (D) and glutamate (E) have negatively charged side chains while lysine (K) and arginine (R) have positively charged side chains; we also mention neutral alanine (A).

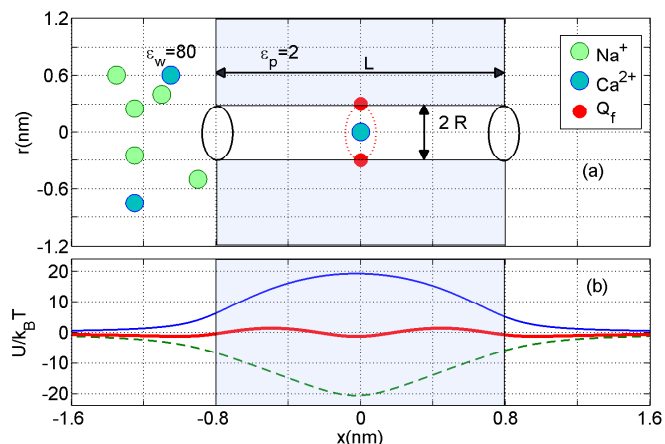


Fig. 1. (Color online) (a) Electrostatic model of a  $\text{Ca}^{2+}$  or  $\text{Na}^+$  channel. Ions move in single file along the channel axis. (b) Energetics of moving  $\text{Ca}^{2+}$  ion for fixed charge  $Q_f = -1e$ . The dielectric self-energy barrier  $U_s$  (full blue line) is balanced by the site attraction  $U_a$  (dashed green line) resulting in a barrier-less energy profile  $U_b$  (red solid line). See text for details.

general physical picture of the phenomena remained unclear.

Here, we reinterpret and generalize the electrostatic analysis of the multi-ion energetics of conduction bands [18] by introducing a novel ionic CB model of conduction and selectivity in biological ion channels thereby bringing them into the context of mesoscopic phenomena. We show that the experimentally-observed valence selectivity phenomena in  $\text{Ca}^{2+}/\text{Na}^+$  channels, including AMFE and mutation-induced transformations of selectivity, and the simulated conduction bands *vs.*  $Q_f$ , can be well-described in terms of CB conductance oscillations while the occupancy represents a Coulomb staircase with Fermi-Dirac (FD) step shapes, so that a ion channel can be thought as a discrete electrostatic device.

In what follows with SI units  $e$  is the proton charge,  $z$  the ionic valence,  $\epsilon_0$  the vacuum permittivity,  $T$  the temperature, and  $k_B$  Boltzmann's constant.

We consider the generic electrostatic model of the SF of a  $\text{Ca}^{2+}/\text{Na}^+$  ion channel shown in Fig. 1. It is described as an axisymmetric, water-filled, cylindrical pore of radius  $R = 0.3\text{nm}$  and length  $L = 1.6\text{nm}$  through a protein hub in the cellular membrane. A centrally-placed, uniform, rigid ring of negative charge  $Q_f$  in the range  $0 \leq |Q_f| \leq 7e$  is embedded

in the wall at  $R_Q = R$ . The left-hand bath, modeling the extracellular space, contains non-zero concentrations of  $\text{Ca}^{2+}$  and/or  $\text{Na}^+$  ions. We take both the water and the protein to be homogeneous continua with relative permittivities  $\epsilon_w = 80$  and  $\epsilon_p = 2$ , respectively, but describe the ions as discrete charges  $q_i = ze$  within the framework of the implicit hydration model moving in single file within the channel, with bulk values of diffusion coefficients  $D_i$ . We take no account of negative counterions inside the SF, which will be few on account of repulsion by the negative  $Q_f$ . The implicit hydration model [10] works well for small  $\text{Ca}^{2+}$  and  $\text{Na}^+$  ions both of which have ionic radii  $R_i \approx 0.1\text{nm}$ .

BD simulations solve the coupled 3D axisymmetrical Poisson electrostatic equation and 1D overdamped Langevin stochastic equation numerically and self-consistently at each simulation step [9], [4], [20]. The model obviously represents a considerable simplification of the actual electrostatics and dynamics of the ions and water molecules moving within the narrow SF [21]. However, reduced models successfully reproduce significant properties of real biological channels [10], [9] thereby illustrating their applicability. Simple models can be also applied to artificial nanopores [16], [12], [21]. Details of the model, its range of validity and its limitations, have been presented and discussed elsewhere [17], [18].

Fig. 1(b) shows the potential energy profiles for a single  $\text{Ca}^{2+}$  ion for the case  $Q_f = -1e$ : a barrier-less effective energy profile appears due to the balance between the dielectric self-energy barrier  $U_s$  (see e.g. [16]) and the site attraction  $U_a$  [18]:

$$U_s = z^2 e^2 / 2C_s, \quad U_a = zeQ_f / C_s. \quad (1)$$

Here,  $C_s = 4\pi\epsilon_0\epsilon_w R^2 / L$  stands for the geometry-depend channel self-capacitance. The captured ion neutralizes  $Q_f$  and restores the effective barrier, thereby preventing the next ion from entering the channel. When  $U_s \gg k_B T$  this amounts to a single-occupancy requirement or *electrostatic exclusion principle*. It plays a significant role in ion permeation and leads to the CB phenomenon, causing the ion channel to behave as single-charge device [14], [15].

The single- and multi-ion conduction bands found in the BD simulations [17], [18] are shown in Fig. 2(a),(b) which plot the  $\text{Ca}^{2+}$  current  $J$  and channel occupancy  $P$  for pure baths of different concentration. Fig. 2(a) shows narrow conduction bands  $M_0, M_1, M_2$  separated by stop-bands of almost zero-conductance centred on the blockade points  $Z_1, Z_2, Z_3$ .

Fig. 2(b) shows that the  $M_n$  peaks in  $J$  correspond to transition regions in channel occupancy, where  $P$  jumps from one integer value to the next, and that the stop-bands correspond to saturated regions with integer  $P = 1, 2, 3, \dots$

Band  $M_0$  corresponds to single-ion barrier-less conduction (see Fig. 1(b)).  $M_1$  corresponds to the double-ion knock-on conduction, which is well-established for L-type  $\text{Ca}^{2+}$  channels [2]; and  $M_2$  corresponds to triple-ion conduction which can be connected with Ryanodine receptor calcium channels [22] (see Table I and related discussion).

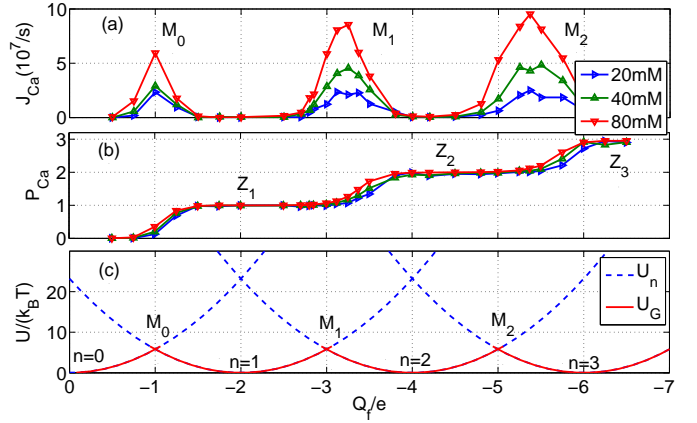


Fig. 2. (Color online) Brownian dynamics simulations of multi-ion conduction and occupancy in a  $\text{Ca}^{2+}$  channel model vs the effective fixed charge  $Q_f$ ; (a),(b) are reworked from [17]. (a) Plots of the  $\text{Ca}^{2+}$  current  $J$  for pure  $\text{Ca}^{2+}$  baths of different concentration (20, 40 and 80mM as indicated). (b) The occupancy  $P$ . (c) The excess self-energy  $U_n$  and ground state energy  $U_G$  vs  $Q_f$  for channels with  $n = 0, 1, 2$  and  $3$   $\text{Ca}^{2+}$  ions inside. The conduction bands  $M_n$  and the blockade/neutralisation points  $Z_n$  are discussed in the text.

We can readily account for the pattern of bands in terms of CB oscillations [13]. The discreteness of the ionic charge allows us to introduce exclusive “eigenstates”  $\{n\}$  of the channel with fixed integer numbers of ions inside its SF having total electrostatic energy  $U_n$ . The transition  $\{n\} \rightarrow \{n+1\}$  corresponds to the entry of a new ion, whereas  $\{n\} \rightarrow \{n-1\}$  corresponds to the escape of a trapped ion. These  $\{n\}$ -states form a discrete exclusive set [23]:

$$n = \{0, 1, 2, \dots\} \quad \sum_n \theta_n = 1; \quad P_c = \sum_n n \theta_n, \quad (2)$$

where  $\theta_n$  is the occupancy of the state  $\{n\}$  and  $P_c$  is the average SF occupancy. In equilibrium  $\theta_n$  is defined by the Boltzmann factor  $\theta_n \propto \exp(-U_n / (k_B T))$ . The exact distribution for  $\theta_n$  and  $P_c$  (which is FD [24], [25]) will be derived below.

The total energy  $U_n$  for a channel in state  $\{n\}$  can be expressed as:

$$U_n = U_{n,s} + U_{n,attr} + U_{n,int} \quad (3)$$

where  $U_{n,s}$  is the self-energy,  $U_{n,attr}$  is the energy of attraction, and  $U_{n,int}$  is the ions’ mutual interaction energy.

We approximate  $U_n$  as the dielectric self-energy  $U_{n,s}$  of the excess charge  $Q_n$  based on the assumption that both the ions and  $Q_f$  are located within the central part of the SF, so that (1) gives the standard CB equation:

$$U_n = Q_n^2 / 2C_s; \quad Q_n = zen + Q_f. \quad (4)$$

Here,  $Q_n$  represents the excess charge at the SF for the  $n$  ions as function of  $Q_f$ . Binomial expansion of  $Q_n^2$  in (4) gives first approximations for  $U_{n,s}$ ,  $U_{n,attr}$  and  $U_{n,int}$  consistent with 1-D Coulomb gas model [16] and with the energetics analysis in [18].

CB appears in low-capacitance systems from quantization of the quadratic energy form (4) at a grid of discrete states

TABLE I  
IDENTIFICATION OF  $\text{Ca}^{2+}$  RESONANT CONDUCTION POINTS  $M_n$  WITH SOME KNOWN CHANNELS AND MUTANTS (EXTENDED FROM [17], [18]).

Channel	Locus	Nominal $Q_f$	Band / Jump	Modelled $Q_f$
Non-selective OmpF [8]	(K)RRRDE	$-1e$	$M_0 \{0 \rightarrow 1\}$	$-1e$
Ca-selective Nav mutant [6]	EEEE	$-3e$	$M_1 \{1 \rightarrow 2\}$	$-3e$
Ca L-type channel [2], Ca-selective OmpF mutant [8]	EEEE	$-4e$	$M_1 \{1 \rightarrow 2\}$	$-3e$
Calcium RyR [22]	DDDD(ED)	$-6e$	$M_2 \{2 \rightarrow 3\}$	$-5e$
Calcium-selective mutants of NavAB [3] and NavChBac [7]	EEEE+DDDD	$-8e$	$M_3 \{3 \rightarrow 4\}$	$-7e$

(2), providing a Coulomb energy gap  $\Delta U_n = U_s$  large enough ( $\Delta U_n \gg k_B T$ ) to block transitions between neighbouring  $\{n\}$  states. We calculate  $U_n$  as a function of  $Q_f$  for  $n = 0, 1, 2, 3$  and focus on the ground state energy  $U_G$  as a function of  $Q_f$ :

$$U_G(Q_f) = \min_n(U_n(Q_f)). \quad (5)$$

Fig. 2(c) plots  $U_n$  and  $U_G$  as functions of  $Q_f$ . We see a periodic pattern with two kinds of  $U_G$  singular points, marked as  $M_n$  and  $Z_n$ . The minima of  $U_G$  (and the blockade regions) appear around the neutralisation points  $Z_n = -zen$  where  $Q_G = 0$  and the occupancy  $P_c$  is saturated at an integer value [16], [18]. For divalent  $\text{Ca}^{2+}$  ions  $\Delta U_n \approx 20k_B T$  and hence CB is strong. The crossover points  $M_n$  ( $U_n = U_{n+1}$ ) allow barrier-less  $\{n\} \rightleftharpoons \{n+1\}$  transitions; they correspond to the  $P_c$  transition regions and to the conduction peaks in  $J$  [18].

The positions of the singular  $Q_f$  points in Fig. 2(c) can be written as:

$$\begin{aligned} Z_n &= -zen \pm \delta Z_n, & \text{Coulomb blockade} \\ M_n &= -ze(n + 1/2) \pm \delta M_n & \text{Resonant conduction} \end{aligned} \quad (6)$$

where  $\delta Z_n, \delta M_n$  are possible corrections for the singular part of the affinity and ion-ion interactions, not accounted for here. Equation (6) is exactly the same as its counterpart in electronic CB. We may therefore interpret the BD-simulated conduction bands (Fig. 2(a)) as CB oscillations of conductance [13] appearing as  $Q_f$  increases and the corresponding occupancy steps (Fig. 2(b)) as a Coulomb staircase [15].

The positions of the  $M_n$  and  $Z_n$  points in the theory (6) and BD simulations (Fig. 2) are consistent with an energetics analysis [18], supporting above interpretation; the deviations in the precise positions of  $M_n$  and  $Z_n$  can be attributed to field leaks and model simplifications.

That is our main result – that the ionic CB model predicts a universal, valence-dependent, periodic pattern of stop/conduction bands similar to the electronic CB oscillations of conductance in quantum dots [13], [15]. It allows us to identify conduction bands with real calcium-conductive channels/mutants.

Table I shows putative identifications of the bands/singularities of the CB model with real channels in the  $\text{Ca}^{2+}/\text{Na}^+$  family, extended from [17], [18]. We identify wild-type calcium channels and  $\text{Ca}^{2+}$ -selective mutants of Na-selective (Nav) channels with the  $\text{Ca}^{2+}$  resonant points  $M_1$  (L-type) and  $M_2$  (RyR). We also identify  $\text{Ca}^{2+}$ -selective mutants of bacterial sodium channels NavChBac [7] and NavAB [3] with point  $M_3$ . In a similar way, we can account for numerous mutation transformations in

$\text{Ca}^{2+}/\text{Na}^+$  channels family, thereby confirming the validity of the CB-based band model. We speculate that the discrepancy between  $Q_f = M_1 = -3e$  derived from CB model and the nominal  $Q_f = -4e$  for the EEEE loci of L-type calcium channels may be associated with protonation [26].

Derivation of the distribution of  $P_c$  in the vicinity of the  $M_n$  points (and hence calculation of the shapes of  $P_c(U_c)$  or  $P_c(Q_f)$ ) follows standard CB theory. For divalent  $\text{Ca}^{2+}$  ions, the Coulomb gap  $\Delta U_n \gg k_B T$  and (2) reduces to a simple 2-state exclusive set:

$$m = \{n, n + 1\}; \quad \theta_n + \theta_{n+1} = 1; \quad P_c = n + \theta_{n+1}. \quad (7)$$

The strong electrostatic exclusion principle (7) plays the same role as the Pauli exclusion principle plays in quantum mechanics [25], [27]. Hence the standard derivation via a partition function, taking account of (7) leads [24] to FD statistics for  $\theta_{n+1}$  and to an excess (fractional) occupancy  $P_c^* = P_c \bmod 1$ :

$$P_c^* = (1 + P_b^{-1} \exp(U_c/k_B T))^{-1}, \quad \text{Fermi-Dirac} \quad (8)$$

where  $U_c = U_{n+1} - U_n$ , and  $P_b$  is a reference occupancy related to the bulk concentration. Note, that (8) is equivalent to the Langmuir isotherm [24] or to Michaelis-Menten saturation. A similar Fermi function was obtained earlier [16] for the variation of  $P_c$  with concentration.

A self-consistent calculation of the conductance can be effected via linear response theory, leading to the standard CB “classical” approximation [13]:

$$J_c/J_{max} = (U_c/k_B T) \sinh^{-1}(U_c/k_B T) \quad (9)$$

where  $J_{max}$  is the barrier-less diffusive current. The current  $J_c$  from (9) exhibits a resonant peak coinciding with the maximum in the derivative of  $P_c$ ,  $dP/dU_c$  (Fig. 3), similar to that of the tunneling current in a quantum dot [13]. The FD function (8) predicts that  $U_c^*/k_B T = -\ln(P_c^*/(1 - P_c^*))$

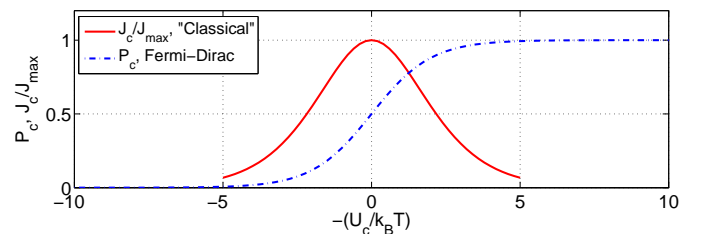


Fig. 3. (Color online) Resonant conduction peak shapes vs  $U_c$  (or equivalently  $Q_f$ ). The occupancy  $P_c$  (blue, dash-dot) shows the Fermi - Dirac transition from  $P_c = 0$  to  $P_c = 1$ . The theoretical current  $J_c/J_{max}$  (red, solid) exhibits a resonant peak in the transitional region.

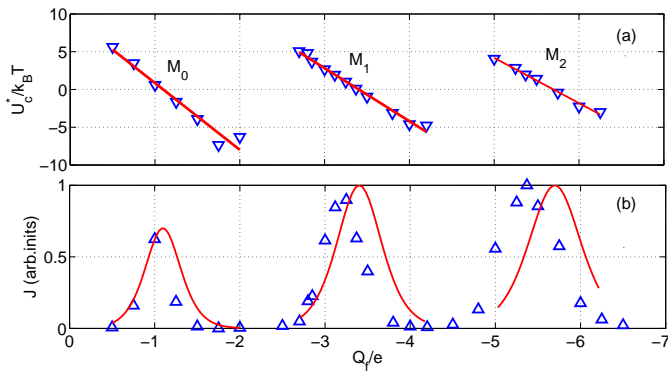


Fig. 4. (Color online) Comparisons of the ionic Coulomb blockade model with Brownian dynamics simulation results as  $Q_f$  is varied. (a) The effective well depth  $U_c^*$  (blue point-down triangles) fitted by Fermi-Dirac function (full red lines). (b) The  $J$  peaks in the “classical” approximation (red solid lines) are compared with simulation results (blue, point-up triangles).

should be linear in  $U_c$  and also (due to the relatively narrow transition region) in  $Q_f$ . Fig. 4(a) plots the predicted sawtooth dependence of  $U_c^*$  on  $Q_f$ , confirming that the  $P_c^*$  transitions obey the FD function (8) of  $U_c$ . Fig. 4(b) compares the CB model with the the BD-simulated  $\text{Ca}^{2+}$  conduction bands  $M_0$ ,  $M_1$ ,  $M_2$  [17]. Theoretical CB oscillations (9) fit the BD-simulated peak shapes and positions reasonably well, given the model simplifications. Although an ion moving inside a channel or nanopore is a classical system described by Newtonian dynamics, it exhibits some quantum-like mesoscopic features [12]. We attribute such behavior to charge discreteness, the electrostatic exclusion principle, and confinement effects.

In conclusion, we have shown that  $\text{Ca}^{2+}$  channel permeation is analogous to mesoscopic transport in quantum dots: the electrostatic exclusion principle leads to an FD distribution of channel occupancy; the stop-bands correspond to blockade; the barrier-less conduction peaks are similar to those in resonant tunneling and can be described by standard CB formulæ. The ionic CB model provides a good account of both the experimental (AMFE and valence selectivity) and the simulated (discrete multi-ion conduction and occupancy bands) phenomena observed in model  $\text{Ca}^{2+}$  channels. The results are should be applicable to other ion channels and to biomimetic nanopores with charged walls.

We are grateful to Aneta Stefanovska, Boris Shklovskii and Max Di Ventra for helpful comments and discussions. The research was supported by the Engineering and Physical Sciences Research Council UK (grant No. EP/M015831/1).

## REFERENCES

- [1] B. Hille, *Ion Channels Of Excitable Membranes*, 3rd ed. Sunderland, MA: Sinauer Associates, 2001.
- [2] W. A. Sather and E. W. McCleskey, “Permeation and selectivity in calcium channels,” *Ann. Rev. Physiol.*, vol. 65, pp. 133–159, 2003.
- [3] L. Tang, T. M. G. El-Din, J. Payandeh, G. Q. Martinez, T. M. Heard, T. Scheuer, N. Zheng, and W. A. Catterall, “Structural basis for  $\text{Ca}^{2+}$  selectivity of a voltage-gated calcium channel,” *Nature*, vol. 505, no. 7481, pp. 56–61, 2014.

- [4] B. Roux, T. Allen, S. Berneche, and W. Im, “Theoretical and computational models of biological ion channels,” *Quart. Rev. Biophys.*, vol. 37, no. 1, pp. 15–103, 2004.
- [5] V. N. Kharkyanen, S. O. Yesylevskyy, and N. M. Berezetskaya, “Approximation of super-ions for single-file diffusion of multiple ions through narrow pores,” *Phys. Rev. E*, vol. 82, p. 051103, 2010.
- [6] S. H. Heinemann, H. Teriau, W. Stuhmer, K. Imoto, and S. Numa, “Calcium-channel characteristics conferred on the sodium-channel by single mutations,” *Nature*, vol. 356, no. 6368, pp. 441–443, 1992.
- [7] L. X. Yue, B. Navarro, D. J. Ren, A. Ramos, and D. E. Clapham, “The cation selectivity filter of the bacterial sodium channel, NaChBac,” *J. Gen. Physiol.*, vol. 120, no. 6, pp. 845–853, 2002.
- [8] H. Miedema, A. Meter-Arkema, J. Wierenga, J. Tang, B. Eisenberg, W. Nonner, H. Hektor, D. Gillespie, and W. Meijberg, “Permeation properties of an engineered bacterial OmpF porin containing the EEEE-luculus of  $\text{Ca}^{2+}$  channels,” *Biophys. J.*, vol. 87, no. 5, pp. 3137–3147, 2004.
- [9] B. Corry, T. Vora, and S. H. Chung, “Electrostatic basis of valence selectivity in cationic channels,” *Biochim. Biophys. Acta-Biomembranes*, vol. 1711, no. 1, pp. 72–86, 2005.
- [10] D. Boda, “Monte Carlo simulation of electrolyte solutions in biology: in and out of equilibrium,” in *Ann. Rep. Comp. Chem.*, ser. Ann. Rep. Comp. Chem., D. Gillespie and N. Baker, Eds. Elsevier, 2014, vol. 10, ch. 5, pp. 127–164.
- [11] B. Corry, “ $\text{Na}^+/\text{Ca}^{2+}$  selectivity in the bacterial voltage-gated sodium channel NavAb,” *PeerJ*, vol. 1, no. DOI10.7717/peerj.16, p. e16 (DOI10.7717/peerj.16), 2013.
- [12] M. Krems and M. Di Ventra, “Ionic Coulomb blockade in nanopores,” *J. Phys. Condens. Matter*, vol. 25, p. 065101, 2013.
- [13] C. W. J. Beenakker, “Theory of Coulomb-blockade oscillations in the conductance of a quantum dot,” *Phys. Rev. B*, vol. 44, no. 4, pp. 1646–1656, 1991.
- [14] M. Stopa, “Rectifying behavior in Coulomb blockades: charging rectifiers,” *Phys. Rev. Lett.*, vol. 88, no. 14, p. 146802, 2002.
- [15] K. K. Likharev, “SET: Coulomb blockade devices,” *Nano et Micro Tech.*, vol. 3, no. 1-2, pp. 71–114, 2003.
- [16] J. Zhang, A. Kamenev, and B. I. Shklovskii, “Ion exchange phase transitions in water-filled channels with charged walls,” *Phys. Rev. E*, vol. 73, p. 051205, 2006.
- [17] I. K. Kaufman, D. G. Luchinsky, R. Tindjong, P. V. E. McClintock, and R. S. Eisenberg, “Multi-ion conduction bands in a simple model of calcium ion channels,” *Phys. Biol.*, vol. 10, no. 2, p. 026007, 2013.
- [18] —, “Energetics of discrete selectivity bands and mutation-induced transitions in the calcium-sodium ion channels family,” *Phys. Rev. E*, vol. 88, no. 5, p. 052712, 2013.
- [19] R. S. Eisenberg, “Atomic biology, electrostatics and ionic channels,” in *New Developments in Theoretical Studies of Proteins*, R. Elber, Ed. Singapore: World Scientific, 1996, pp. 269–357.
- [20] C. Berti, S. Furini, D. Gillespie, D. Boda, R. S. Eisenberg, E. Sangiorgi, and C. Fiegna, “Three-dimensional Brownian dynamics simulator for the study of ion permeation through membrane pores,” *J. Chem. Theor. Comp.* dx.doi.org/10.1021/ct4011008, 2014.
- [21] A. Laio and V. Torre, “Physical origin of selectivity in ionic channels of biological membranes,” *Biophys. J.*, vol. 76, no. 1, pp. 129–148, 1999.
- [22] D. Gillespie, “Energetics of divalent selectivity in a calcium channel: The ryanodine receptor case study,” *Biophys. J.*, vol. 94, no. 4, pp. 1169–1184, 2008.
- [23] P. H. Nelson, “A permeation theory for single-file ion channels: One- and two-step models,” *J. Chem. Phys.*, vol. 134, pp. 165 102–165 114, 2011.
- [24] R. H. Fowler, “A statistical derivation of Langmuir’s adsorption isotherm,” in *Mathematical Proceedings of the Cambridge Philosophical Society*, vol. 31. Cambridge: CUP, 1935, pp. 260–264.
- [25] G. Kaniadakis and P. Quarati, “Kinetic equation for classical particles obeying an exclusion principle,” *Phys. Rev. E*, vol. 48, no. 6, pp. 4263–4270, 1993.
- [26] S. Furini, P. Barbini, and C. Domene, “Effects of the protonation state of the EEEE motif of a bacterial  $\text{Na}^+$ -channel on conduction and pore structure,” *Biophys. J.*, vol. 106, pp. 2175–2183, 2014.
- [27] J.-L. Liu and R. Eisenberg, “Correlated ions in a calcium channel model: A Poisson-Fermi theory,” *J. Phys. Chem. B*, vol. 117, pp. 12 051–12 058, 2013.